J. Fluid Mech. (2012), *vol.* 691, *pp.* 392–416.
doi:10.1017/jfm.2011.480

The rise heights of low- and high-Froude-number turbulent axisymmetric fountains

H. C. Burridge and G. R. Hunt†

Department of Civil and Environmental Engineering, Imperial College London, Imperial College Road, London SW7 2AZ, UK

(Received 15 July 2011; revised 30 September 2011; accepted 27 October 2011; first published online 12 December 2011)

We present the results of an experimental investigation across a broad range of source Froude numbers, $0.4 \leqslant Fr_0 \leqslant 45$, into the dynamics, morphology and rise heights of Boussinesq turbulent axisymmetric fountains in quiescent uniform environments. Typically, these fountains are thought to rise to an initial height, z_i, before settling back and fluctuating about a lesser (quasi-) steady height, z_{ss}. Our measurements show that this is not always the case and the ratio of the fountain's initial rise height to steady rise height, $\lambda = z_i/z_{ss}$, varies widely, $0.5 \lesssim \lambda \lesssim 2$, across the range of Fr_0 investigated. As a result of near-ideal start-up conditions provided by the experimental set-up we were consistently able to form a vortex at the fountain's front. This enabled new insights into two features of the initial rise of turbulent fountains. Firstly, for $1.0 \lesssim Fr_0 \lesssim 1.7$ the initial rise height is *less* than the steady rise height. Secondly, for $Fr_0 \gtrsim 5.5$, the vortex formed at the fountain's front pinches off, separates from the main body and rises high above the fountain; there is thus a third rise height to consider, namely, the maximum vortex rise height, z_v. From our observations we propose classifying turbulent axisymmetric fountains into five regimes (as opposed to the current three regimes) and present detailed descriptions of the flow in each. Finally, based on an analysis of the rise height fluctuations and the width of fountains in (quasi-) steady state we provide further insight into the physical cause of height fluctuations.

Key words: plumes/thermals, turbulent convection

1. Introduction

Dense turbulent fountains formed as fluid is ejected energetically vertically upwards from an axisymmetric source into quiescent uniform environments initially exhibit a jet-like behaviour as they rise. However, being denser than the ambient the rising flow is slowed by gravity and this decreasing vertical velocity combined with the entrainment of external ambient fluid forms the cone-like shape classically associated with starting fountains (Turner 1966). The fountain continues to rise until the opposing momentum flux, arising from the work done by the fluid's negative buoyancy, balances at the fountain's top with the momentum flux from the source; at this instant the fountain has reached its initial rise height, z_i. A downflow then forms around the upflowing core and the momentum exchanged between these two flows reduces the

† Email address for correspondence: gary.hunt@imperial.ac.uk

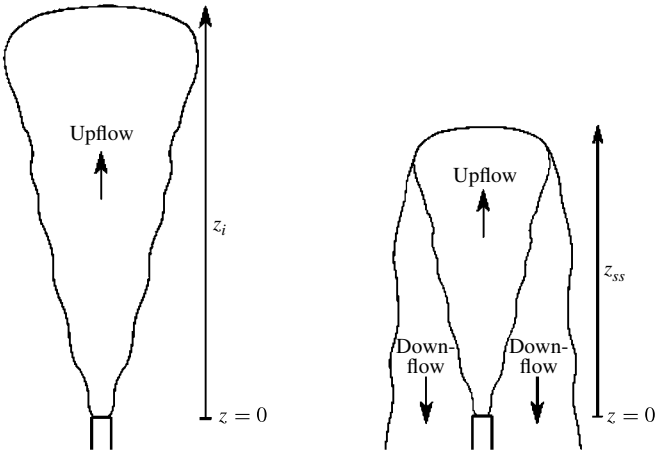

FIGURE 1. Schematic of a relatively high-Froude-number fountain at initial rise height, z_i, and subsequent lesser steady rise height, z_{ss}.

vertical extent of the rising core. Rise heights are then observed to fluctuate about a lesser steady height, z_{ss}, and the fountain is described as being in a quasi-steady state. Figure 1 shows schematics of one such energetic fountain both at the initial rise height and during the subsequent steady state. Whilst we have described the flow of a heavy fluid being forced vertically upwards, for Boussinesq fountains the same dynamics apply and similar flows are observed should a light fluid be forced downwards.

The occurrence of fountains within nature and their applications in industry are wide and diverse. These include: plumes rising in a stratified environment (Devenish, Rooney & Thompson 2010), flows in volcanic magma chambers (Campbell & Turner 1989), the heating of large industrial spaces (Baines, Turner & Campbell 1990), building ventilation by underfloor air distribution systems (Liu & Linden 2006), the discharge of brine from desalination plants (Zhang & Baddour 1998) and the compensation of fuel tanks within naval ships (Friedman & Katz 1999).

By their very nature, turbulent fountains are complex flows and their current classification (Kaye & Hunt 2006) is based on the changing dependence of their rise heights on the source Froude number, Fr_0. The initial rise height for very low source Froude numbers follows the relationship $z_i/r_0 \propto Fr_0^{2/3}$, where r_0 is the radius of the fountain's source at $z = 0$. With increasing Froude number the initial rise height sensitivity to Fr_0 increases so that $z_i/r_0 \propto Fr_0^2$ and then decreases for fountains of even higher source Froude number for which $z_i/r_0 \propto Fr_0$. These changes in rise height dependence on Fr_0 form the basis for the classification of fountains into the three regimes (very weak, weak and forced) and reflect how the dominant physical processes alter with increasing Fr_0. This raises the question of whether the ratio of the initial rise height, z_i, to the steady rise height, z_{ss}, varies with Fr_0 as it is not clear why a constant rise height ratio, $\lambda = z_i/z_{ss} = 1.43$ as reported for 'forced' fountains (Turner 1966), should apply across the entire range of Fr_0. One might reasonably anticipate a dependence of λ on Fr_0, particularly when one considers that, for example, the physics of a low-source-Froude-number (very weak) fountain differs significantly from that of high-source-Froude-number (forced) fountain, the former having been successfully modelled as a hydraulic flow over a weir (the fountain nozzle being the weir, Kaye & Hunt 2006) and the latter by reversing the sign of the source buoyancy

flux relative to momentum flux in classical plume theory. Whilst our experimental measurements (§ 3) of high-Froude-number fountains independently confirm Turner's findings, we show that the rise height ratio is not constant and varies by a factor of four, $0.5 \lesssim \lambda \lesssim 2$ for $0.4 \leqslant Fr_0 \leqslant 45$.

Turner deduced on dimensional grounds that the initial rise height, scaled on the source radius, is directly proportional to the source Froude number ($z_i/r_0 \propto Fr_0$); the Froude number is defined as $Fr_0 = w_0/\sqrt{r_0\, g_0'}$, where w_0 is the vertical source velocity and $g_0' = g(\rho_0 - \rho_a)/\rho_a$ the source reduced gravity, with ρ_0 and ρ_a denoting the density of the source and ambient fluids, respectively. Turner verified this linear power-law dependence by comparison with rise height measurements of saline fountains from circular nozzles. These fountains, now recognised as 'forced' fountains, rose to an initial maximum height before the subsequent exchange of momentum between the upflow and downflow reduced the vertical extent to a quasi-steady height for which $\lambda = z_i/z_{ss} \approx 1.43$. Turner's experiments covered the range $0.55 < Fr_0 < 11.8$ and notably no dependence of the rise height ratio on Fr_0 was identified.

Theoretical descriptions of the bulk dynamics of forced fountains, up to their initial maximum rise height and prior to interaction between the upflowing core and the downflowing perimeter, have been successfully developed using the Morton, Taylor & Turner (1956) plume theory and extensions of it (e.g. McDougall 1981). The adoption of an entrainment coefficient, α, suitable for a highly forced plume, e.g. $\alpha = 0.058$ recommended by Kaye & Hunt (2006), enables good prediction of the initial rise height. The agreement with measurement as achieved with this entrainment coefficient is understandable when one considers that for high-Fr_0 sources the majority of the rise height occurs over a momentum-jet length scale.

Following the experimental work of Turner (1966), a succession of authors (including Baines *et al.* 1990; Bloomfield & Kerr 1998; Zhang & Baddour 1998; Ansong, Kyba & Sutherland 2008; Williamson *et al.* 2008) made measurements of fountain rise heights which now encompass very weak, weak and forced releases. The transition between very weak and weak fountains is generally accepted as $Fr_0 \approx 1$ and whilst the work of Zhang & Baddour (1998) cites the transition between weak and forced fountains as $Fr_0 \approx 7$, later works cite the transition as $Fr_0 \approx 3$ (e.g. Kaye & Hunt 2006). The experimental work of Zhang & Baddour (1998) focused on classifying fountains into two regimes, weak and forced. Their data support a linear rise height dependence on Fr_0 for $Fr_0 \gtrsim 4$, albeit at a lesser gradient than that of higher-Fr_0 fountains.

The need for the three regimes can be deduced by consideration of the three characteristic length scales that naturally arise from a source from which there are steady fluxes of volume ($Q_0 \propto r_0^2 w_0$), momentum ($M_0 \propto r_0^2 w_0^2$) and buoyancy ($B_0 \propto r_0^2 w_0 g_0'$). For forced fountains, momentum and buoyancy fluxes dominate and as such the initial rise height is expected to scale on the momentum jet length (Turner 1966)

$$z_i \propto M_0^{3/4}/B_0^{1/2} \propto r_0^{1/2} w_0/g_0'^{1/2} = r_0 Fr_0. \tag{1.1}$$

For weak fountains, all three fluxes are of importance giving

$$z_i \propto M_0^2/B_0 Q_0 \propto w_0^2/g_0' = r_0 Fr_0^2. \tag{1.2}$$

For very weak fountains, the fountain is hydraulically controlled at the source giving

$$z_i \propto Q_0^{1/3} M_0^{1/3}/B_0^{1/3} \propto r_0^{2/3} w_0^{2/3}/g_0'^{1/3} = r_0 Fr_0^{2/3}. \tag{1.3}$$

For a given fountain, the local Froude number, $Fr(z)$, decreases with height z from $Fr = Fr_0$ at $z = 0$ to $Fr = 0$ at the fountain-top. Thus during its initial rise a forced fountain has a region where $Fr(z)$ decreases from the source value to values characteristic of weak fountains, before decreasing further to values characteristic of very weak fountains. The relative fountain heights at which the local Froude number reaches the transitional values between the three regimes are outlined in Appendix.

Experimental measurements have been complemented by numerous further advances in the theoretical and numerical modelling of turbulent fountains. Numerical studies include work investigating weak fountains (Lin & Armfield 2000*a*,*b*), starting fountains (Marugán-Cruz, Rodríguez-Rodríguez & Martínez-Bazán 2009; Wang, Law & Adams 2011), laminar to turbulent transitional fountains (Williamson, Armfield & Lin 2010), fountain-top entrainment (Devenish *et al.* 2010) and the internal dynamics of fountains (Williamson, Armfield & Lin 2011). Theoretical works have sought to include the interaction between upflow and downflow (McDougall 1981; Bloomfield & Kerr 2000) and fountain classification (Kaye & Hunt 2006). The theoretical study of Carazzo, Kaminski & Tait (2010), through the development of a Reynolds-averaged integral model, yields a framework providing an explicit expression for the fountain entrainment coefficient both during the initial rise, α_i, and whilst in steady state, α_{ss}. The rise height ratio was then deduced to be of the form $\lambda = z_i/z_{ss} \propto \sqrt{\alpha_{ss}/\alpha_i}$. Carazzo *et al.* (2010) were unable to validate this result by comparison with measurements due to a lack of information in the literature on the rise height variation between initial and steady heights.

In our paper we address this issue. We raise the question of what is the variation of initial and steady rise heights across a range of Fr_0 encompassing forced, weak and very weak fountains. A description of our experimental apparatus and measurement techniques is given in § 2. We present rise height measurements, focusing on relatively high source Reynolds numbers, $Re_0 = w_0\, r_0/\nu_0$ (ν_0 denoting the kinematic viscosity of the source fluid). We follow this with our results (§ 3) which show the variation of λ with Fr_0 and we identify a number of new features distinct to a range of source Froude numbers within the current classification. At low Fr_0 we observe that an initial local (in time) maximum rise height is reached before the symmetry of the flow breaks down and greater rise heights are subsequently obtained. This finding challenges the notion that fountains rise to an initial maximum height prior to the development of a counterflow and thereafter fluctuate about a lower steady rise height. With increasing Fr_0 we observe significant differences in rise height ratio and in the manner in which the rise heights are attained. Moreover for $Fr_0 \gtrsim 5.5$, a vortex formed at the fountain's front during the initial transients, pinches off the main body of the fountain and rises significantly higher; as a consequence there are then two initial rise heights to consider. For $1.7 \lesssim Fr_0 \lesssim 5.5$ the fountain's head, although remaining integral to the fountain, has a significant role in determining the dynamics of the initial rise. Based on our observations and measurements of distinct rise height behaviours we propose a new fountain classification comprising five types. In § 5 we summarize our findings and present our conclusions.

2. Experiments

2.1. *Set-up*

Saline solution driven by an ISMATEC MCP-Z Process gear pump, at volume flow rates of $15\ \mathrm{cm^3\ s^{-1}} \leqslant Q_0 \leqslant 65\ \mathrm{cm^3\ s^{-1}}$, was ejected vertically upwards through a smooth-bore cylindrical nozzle into a clear glass-sided visualization tank, of horizontal

cross-section 176 cm × 125 cm, containing fresh water to a depth of 120 cm. The nozzle was aligned vertically and rigidly clamped in place within the visualization tank. Nozzles of internal radii $r_0 = 0.51, 0.75$ and 1.1 cm and of lengths exceeding $36r_0$ (to ensure the internal flow was fully developed at the nozzle exit, White 2003) were used. To ensure that fluid entrained by the fountains was solely of ambient density the nozzle exit (at $z = 0$) was never less than $80r_0$ from the base of the tank and the tank was emptied before the saline layer (that accumulated at the base of the tank) exceeded a depth of $70r_0$. For the large majority of experiments reduced gravities of 15 cm s^{-2} $\leqslant g_0' \leqslant$ 30 cm s^{-2} were used. However, to achieve the low Fr_0 required for very weak fountains whilst maintaining suitably high Reynolds numbers (see § 2.3), reduced gravities of up to $g_0' \approx 150$ cm s^{-2} were required. Prior to release the saline solution was stored in an 80 l reservoir which was connected to the nozzle, via the gear pump, using reinforced PVC tubing. The saline reservoir was permanently immersed within the visualization tank to equalize the temperatures of the saline solution and the ambient; their densities were measured using an Anton PAAR DMA 4500 densitometer to an accuracy of $\pm 5 \times 10^{-5}$ g cm^{-3}.

The fountain was made visible by staining the source fluid with methylene blue to a concentration of approximately 0.01 mg cm^{-3}. The apparatus was diffusively back-lit using a light box containing an array of high-frequency fluorescent tubes. Images of the experiments were recorded as 8-bit bitmap image files at a frequency of 24 frames per second and digitally stored via a computer-controlled BitFlow R3 frame grabber card. Images were captured using a JAI CVM4^{+}CL camera, resolution 1372 (h) × 1024 (v), with a Pentax 12.5–75 mm 1:1.8 TV ZOOM lens and a Hoya R(25A) red filter.

2.2. *Diagnostics*

A digitized movie was produced of each experiment by assembling the captured images within Matlab (R2010b). From each movie a time series of vertical light intensity was created in order to establish the variation in rise height. Averaging the pixel light intensities horizontally across each image produced a vertical bar of pixels. Aligning side-by-side the vertical pixel bar from each image produced a time series of rise heights for each fountain. The first image in figures 6, 8, 9, 10 and 12 (§ 3) shows these time series. The height of the fountain's top, $z_f(t)$, was then followed to ascertain the initial rise height, z_i, and the mean steady-state rise height, z_{ss}. Similarly, tracking the vortex height, $z_v(t)$, yielded the maximum vortex rise height, z_v. The rise velocity of the fountain's top, $w_f(t) = \mathrm{d}z_f/\mathrm{d}t$, and of the vortex, $w_v(t) = \mathrm{d}z_v/\mathrm{d}t$, were then attained. Measurements of the fountain's breadth were made by analysing, within every frame, each pixel row and locating the left-hand and right-hand edges of the fountain; the distance between edges being taken as the breadth, denoted $2b(z, t)$, at a given height and time. Thus for each experiment we also obtained a time series of fountain breadth at all heights. Figure 2 shows images and an outline of a fountain with the relevant heights and breadths marked, including those introduced later in this section.

Each experiment was recorded for a time interval $[0, T_2]$ of duration varying from 150 to 420 s. The time interval over which measurements were recorded whilst the fountain was in steady state $[T_1, T_2]$ yielded the statistics used, including the mean steady-state rise height,

$$z_{ss} = \frac{1}{T_2 - T_1} \int_{T_1}^{T_2} z_f(t)\, \mathrm{d}t. \tag{2.1}$$

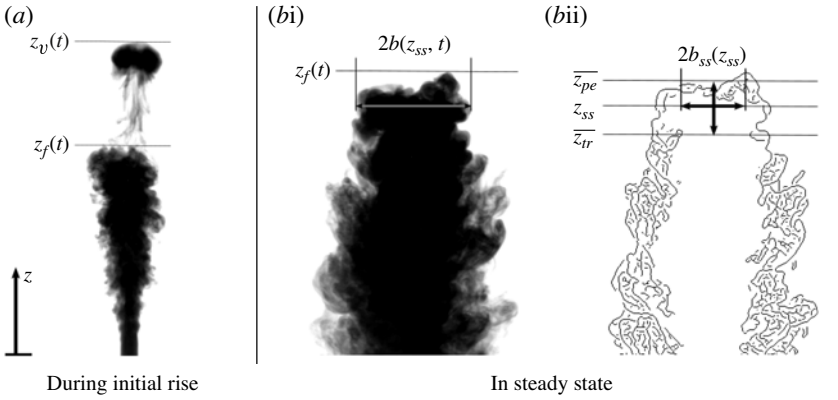

FIGURE 2. The same highly forced fountain at two different instants during experimentation; the outline (*b*ii) shows the edges identified from (*b*i). Marked on (*a*) and (*b*i) are the instantaneous breadths and heights. Marked on (*b*ii) are the statistically generated breadths and heights for the experiment pictured, with the vertical and horizontal arrows showing the scale of $(\overline{z_{pe}} - \overline{z_{tr}})$ and $2b_{ss}(z_{ss})$ (as defined in (2.3) and (2.4)), respectively.

The interval $[T_1, T_2]$ needed to be sufficiently long to ensure that the measured mean, z_{ss}, was a good estimate of the true mean rise height, μ_{ss}; the true mean being that for an experiment run indefinitely. To ensure our recording intervals were sufficiently long we calculated an estimate of the mean-square error, $\mathbb{E}[(\mu_{ss} - z_{ss})^2]$, of our measurements

$$\mathbb{E}[(\mu_{ss} - z_{ss})^2] \approx \frac{2\sigma_{ss}^2}{T_2 - T_1} \int_{T_1}^{T_2} R(\tau)\, \mathrm{d}t, \tag{2.2}$$

see Tennekes & Lumley (1972), where σ_{ss}^2 is the variance of $z_f(t)$ in the interval $[T_1, T_2]$ and $R(\tau)$ the autocorrelation coefficient. For all experiments the duration of recording was increased until $\sqrt{\mathbb{E}[(\mu_{ss} - z_{ss})^2]}/z_{ss} \lesssim 0.5\,\%$, thereby ensuring any bias in the measured mean value of z_{ss} due to the recording time was small and comparable across the range of Fr_0 considered.

To quantify the scale of fountain height fluctuations (for $t > T_1$) it was necessary to define measures of the fountain's mean 'peak' height, $\overline{z_{pe}}$, and mean 'trough' height, $\overline{z_{tr}}$, figure 2, which were insensitive to statistical outliers and to the time interval $[T_1, T_2]$, namely

$$\overline{z_{pe}} = \frac{1}{T_{pe}} \int_{T_1}^{T_2} z_{pe}(t)\, \mathrm{d}t, \quad \overline{z_{tr}} = \frac{1}{T_{tr}} \int_{T_1}^{T_2} z_{tr}(t)\, \mathrm{d}t \tag{2.3}$$

where $z_{pe}(t) = z_f(t)$ for $z_f(t) \geqslant z_{ss} + \sigma_{ss}$, otherwise $z_{pe}(t) = 0$, and T_{pe} is the total length of time for which $z_f(t) \geqslant z_{ss} + \sigma_{ss}$; $z_{tr}(t) = z_f(t)$ for $z_f(t) \leqslant z_{ss} - \sigma_{ss}$, otherwise $z_{tr}(t) = 0$, and T_{tr} is the total length of time for which $z_f(t) \leqslant z_{ss} + \sigma_{ss}$.

As a measure of the fountain-top width we define

$$2b_{ss}(z_{ss}) = \frac{2}{T_h} \int_{T_1}^{T_2} b'(t, z_{ss})\, \mathrm{d}t \tag{2.4}$$

where $b'(t, z_{ss}) = b(t, z_{ss})$ when $z_f(t) \geqslant z_{ss}$, otherwise $b'(t, z_{ss}) = 0$, and T_h is the total length of time for which $z_f(t) \geqslant z_{ss}$.

2.3. *Source conditions and start-up*

Our experiments investigated source Froude numbers in the range $0.4 \lesssim Fr_0 \lesssim 45$, the upper limit being the maximum achievable with our experimental apparatus. However, no qualitative change in fountain behaviour above this limit has been reported elsewhere nor is any anticipated.

The pinch-off of a vortex at the fountain's front for $Fr_0 \gtrsim 5.5$ and the subsequent maximum rise height, z_v, of the vortex was of particular interest to us. Forming the separating vortex in a repeatable fashion was experimentally problematic and a broad spread of z_v was measured even between nominally identical experiments. The vortex rise and its general behaviour was sensitive to Fr_0 and Re_0, the initial acceleration of the source fluid by the pump, the density interface at the nozzle exit (at $t = 0$) and any residual motion in the visualization tank. We now consider these aspects in turn.

For in excess of 80 % of all experiments presented herein the gear pump set-up (unrestricted by the need to include a flow meter) accelerated source fluid from rest to the desired velocity (and hence Fr_0) within a 'ramp-up' time of $t_r \leqslant 1/24$ s, where $1/24$ s was the frame rate of the camera. Thus within a single frame the desired Fr_0 was consistently attained thereby allowing the repeatable formation of an initial vortex. A survey of existing literature reveals that this was not the case in a number of other experimental studies on fountains and in fact very few details regarding the ramp-up can be found. For studies where the ramp-up time (i.e. the time for the Froude number at the source to reach the desired value Fr_0) was significant the fountain would not necessarily attain the full initial height, z_i, nor would the initial vortex form. For example, should the flow of source fluid be started gradually, such that the time to reach Fr_0 was comparable to the time for the returning downflow to develop, then the initial height would be decreased by the momentum exchange between the upflow and the downflow and $z_i \to z_{ss}$. In other words the parameter t_r/t_i, where t_i denotes the time at which the fountain reaches initial rise height, whilst previously unconsidered in experimental work, can have a profound influence on rise heights. To ensure the fountains we produced were also of suitably high source Reynolds numbers, low volume flow rates were avoided whenever possible and the pump's maximum flow rate was often used. For experimental configurations where the pump flow rate was close to maximum, the pump took up to 1/8 s to achieve the desired flow rate. To ensure that the ramp-up time never significantly affected the initial rise dynamics we monitored t_r/t_i. The worst case from any of the experiments performed gave $t_r/t_i \approx 0.3$, whilst for in excess of 90 % of all experiments $t_r/t_i < 0.1$.

To ensure the observed trends in rise height fluctuations (§ 3) were not due to time-varying source conditions, a set of calibration tests were carried out. An individual calibration test (for every value of volume flow rate used) recorded the actual volume flow rate supplied by the pump, $Q_0(t)$, for the given dialled input volume flow rate. For comparison we define similar statistics to (2.3) for the 'peak' and 'trough' mean volume flow rates supplied: $\overline{Q_{pe}}$ denotes the mean observed value for $Q_{pe}(t)$, where $Q_{pe}(t) = Q_0(t)$ for $Q_0(t) \geqslant \overline{Q_0(t)} + \sigma_{Q_0}$; and $\overline{Q_{tr}}$ denotes the mean observed value of $Q_{tr}(t)$, where $Q_{tr}(t) = Q_0(t)$ for $Q_0(t) \leqslant \overline{Q(t)} - \sigma_{Q_0}$, where σ_{Q_0} is the standard deviation of the measured flow rate. Notably, flow rate variations were nominally constant with fluctuations of typically 2 %.

Williamson *et al.* (2008) report $Re_0 = 120$ to be the start of the transition to turbulence for fountains, whilst fountains with $Re_0 \gtrsim 2000$ are reported therein to be fully turbulent. For fountains of a given reduced gravity and source

radius, $Fr_0 \propto Re_0$. Thus, producing fully turbulent low-Froude-number Boussinesq fountains is experimentally more problematic. Fountains studied herein were typically of source Reynolds number $Re_0 \gtrsim 2000$. Where this was not possible a number of different source Reynolds numbers were examined for a given source Froude number to highlight any dependence of fountain rise heights on Re_0 (see § 3.2 for further details).

The interval between experiments needed to be sufficiently long to ensure the ambient was quiescent, whilst not so long as to allow diffusion to compromise the sharp density interface between the ambient and source fluids at the nozzle exit. Consideration of two characteristic time scales, a settling time scale (t_q), and a diffusive time scale (t_l), enabled suitable times between experiments to be determined. The diffusive time scale $t_l = \mathscr{L}^2/2\mathscr{D} \approx 400$ s, where the diffusivity of salt in water $\mathscr{D} = 1.25 \times 10^{-5}$ cm^2 s^{-1} (Washburn 2003) and we have taken $\mathscr{L} = 0.1$ cm (the accuracy to which heights were recorded). The settling time scale, found to be in the range 290 s $\lesssim t_q \lesssim$ 6000 s was taken as the ratio of the square of the fountain's maximum radius and the viscosity of the ambient; the fountain's maximum radius being a characteristic length scale for the distance over which viscosity must act to quiesce the ambient. For fountains where the settling time scale exceeded the diffusive time scale the tank was allowed to settle for a sufficiently long time to allow the ambient to quiesce before purging, at very low flow rates, the plug of diffuse fluid from the nozzle. The tank was then left for a shorter time period before the next experiment commenced.

3. Results

We begin with a brief synopsis of our findings before discussing our results in detail in §§ 3.1–3.4. For forced fountains our measurements confirm the rise height ratio and scalings of Turner (1966). However, we note the presence of distinct vortices in the initial formation and subsequent rise to an initial maximum height, which greatly alter the rise dynamics, particularly for $Fr_0 \gtrsim 5.5$. In addition, our results for the steady-state rise heights agree well with the scalings described in Kaye & Hunt (2006) across the range of source Froude numbers we have investigated.

For fountains of relatively low source Froude number, $1.0 \lesssim Fr_0 \lesssim 1.7$, we observe that the initial rise height is not the maximum rise height and, moreover, within this range of Fr_0 we identify fountains where the rise height ratio is below unity.

The formation or otherwise of a vortical structure at the fountain's front is central to our revised fountain classification as it influences not only the initial rise height but the entire morphology of the fountain during the initial rise. These initial vortices were formed repeatably by achieving close to ideal initial conditions (§ 2.3) through ensuring a uniform quiescent ambient, a sharp density interface at the nozzle exit and the rapid acceleration of the source fluid. For $1.7 \lesssim Fr_0 \lesssim 2.8$ the formation of the vortical structure is apparent but it remains integral to the fountain (figure 9(*d*). For $2.8 \lesssim Fr_0 \lesssim 5.5$ the vortex remains attached yet is clearly distinguishable from the fountain body (figure 8*c–f*). For still higher source Froude number, $Fr_0 \gtrsim 5.5$, the vortex separates from the main body of the fountain and rises high above (figure 6*c–f*).

These features lead us to propose a new fountain classification consisting of five classes. The current classification and the primary distinctions leading to our proposed classification are illustrated in figure 3. Each of the classes is distinguished as follows: (*a*) for $Fr_0 \lesssim 1.0$ the source forcing is only sufficient to generate a weir-like flow

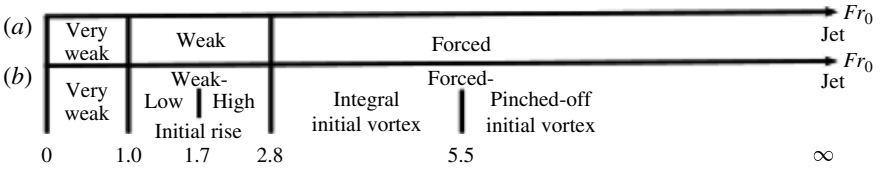

FIGURE 3. (*a*) Current fountain classification and (*b*) the distinguishing feature of each of the five classes within the new proposed fountain classification.

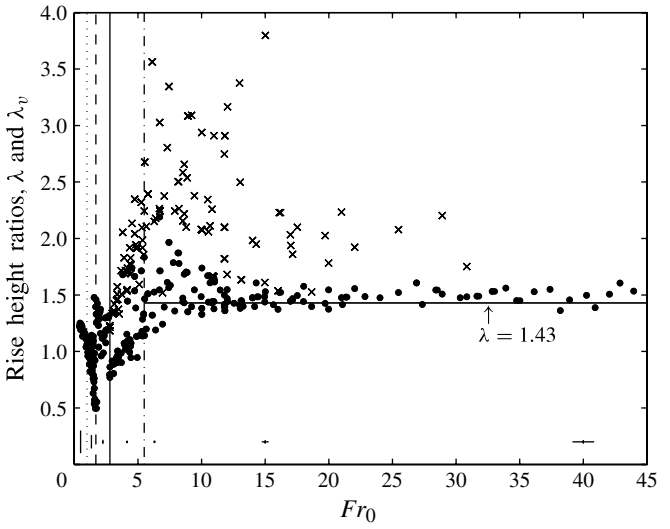

FIGURE 4. Rise height ratio variation with Fr_0: measurements of $\lambda = z_i/z_{ss}$ (•) and $\lambda_v = z_v/z_{ss}$ (×). The vertical dotted line marks the very weak-to-weak transition, dashed line marks the weak-to-intermediate transition, solid line marks the intermediate-to-forced transition and dashed-dotted line marks the forced-to-highly forced transition. Seven error bars (aligned along $\lambda = 0.2$) are plotted to indicate the maximum error associated with an experiment in that region of Fr_0. An exploded view highlighting trends for $Fr_0 \leqslant 7$ is shown in figure 14 and is discussed in § 3.3.

– herein *very weak fountains*; (*b*) for $1.0 \lesssim Fr_0 \lesssim 1.7$ the weak source forcing leads to 'low' initial rise heights – herein *weak fountains*; (*c*) for $1.7 \lesssim Fr_0 \lesssim 2.8$ the relatively weak forcing produces 'high' initial rise heights – herein *intermediate fountains*; (*d*) for $2.8 \lesssim Fr_0 \lesssim 5.5$ the relatively strong forcing forms a distinct yet integral initial vortex – herein *forced fountains* and (*e*) for $Fr_0 \gtrsim 5.5$ the strong forcing forms an initial vortex which pinches off – herein *highly forced fountains*.

In figures 4, 7, 11, 14, 15 and 16 vertical lines mark the boundaries between these fountain classes; dotted lines mark the very weak-to-weak transition, dashed lines mark the weak-to-intermediate transition, solid lines mark the intermediate-to-forced transition and dashed-dotted lines mark the forced-to-highly forced transition. In addition, error bars (at specified vertical locations) are plotted at Fr_0 values such that the vertical and horizontal extent of the bars illustrate the maximum error associated with any experiment in that region of Fr_0 values.

Significantly, our results show that the rise height ratio, other than for highly forced fountains, is not constant at $\lambda = 1.43$. This is clear from figure 4 which also shows

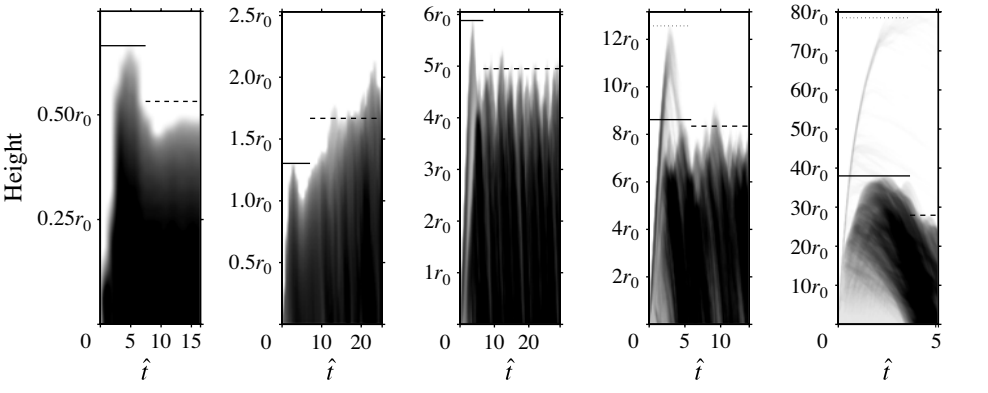

FIGURE 5. Time series for five qualitatively different fountains illustrating the initial rise height z_i (—), steady rise height z_{ss} (- - -) and where applicable (*d*,*e*) vortex rise height z_v(· · ·). $\hat{t} = tg_0^{'}/w_0$.

that the ratio of the vortex rise height to the steady rise height, $\lambda_v = z_v/z_{ss}$ (relevant only to forced and highly forced fountains, marked ×) varies widely. It is noted that whilst the initial vortex formed and separated from the fountain for the highest Fr_0 examined the depth of the visualization tank prevented vortex rise heights being recorded for fountains of $Fr_0 \gtrsim 30$.

3.1. *Morphology and dynamics*

For all fountains we observed that fluid first ejected from the nozzle formed a domed cap. The subsequent dynamics varied widely depending on Fr_0 and the following subsections document the rise and fall behaviours observed and measured over the range of Fr_0 indicated. These contrasting behaviours, as highlighted in the time series of figure 5, form the basis for the extended classification. Behaviours are described for decreasing Fr_0 (§ 3.1.1 to § 3.1.5) beginning with highly forced fountains.

3.1.1. *Highly forced fountains,* $Fr_0 \gtrsim 5.5$

A circulation of fluid within the domed starting cap was clearly visible; figure 6 images Ex(*a*) and Ex(*b*) show the vortical cap atop the fountain stem. Trailing in the lee of this lead vortex, a number of smaller vortices formed along the stem of fluid linking the lead vortex to the nozzle (figure 6*b* and Ex(*b*)) giving the stem a ribbed outline. The lead vortex subsequently pinched off and rose separately above the main body of the fountain. We therefore distinguish between the position of the highest point on the vortex, $z_v(t)$, and the highest point on the body of the fountain, $z_f(t)$.

Prior to pinching off, fluid was ejected periodically from the lead vortex and this fluid descended around the rising stem. The smaller vortices aligned along the stem appeared to instantaneously break down causing the entire stem to depart from an ordered, ribbed appearance (figure 6*b*) to a stem characterized by numerous smaller-scale turbulent eddies (figure 6*c*). The fountain body continued to rise, albeit more slowly, forming the classical cone-like fountain shape (figure 6*d*). The now turbulent fountain was clearly entraining ambient fluid (observable from the opacity of the fluid at the fountain's edge) prior to the body reaching its initial rise height. This initial rise height was the absolute maximum height reached by the main fountain body – the

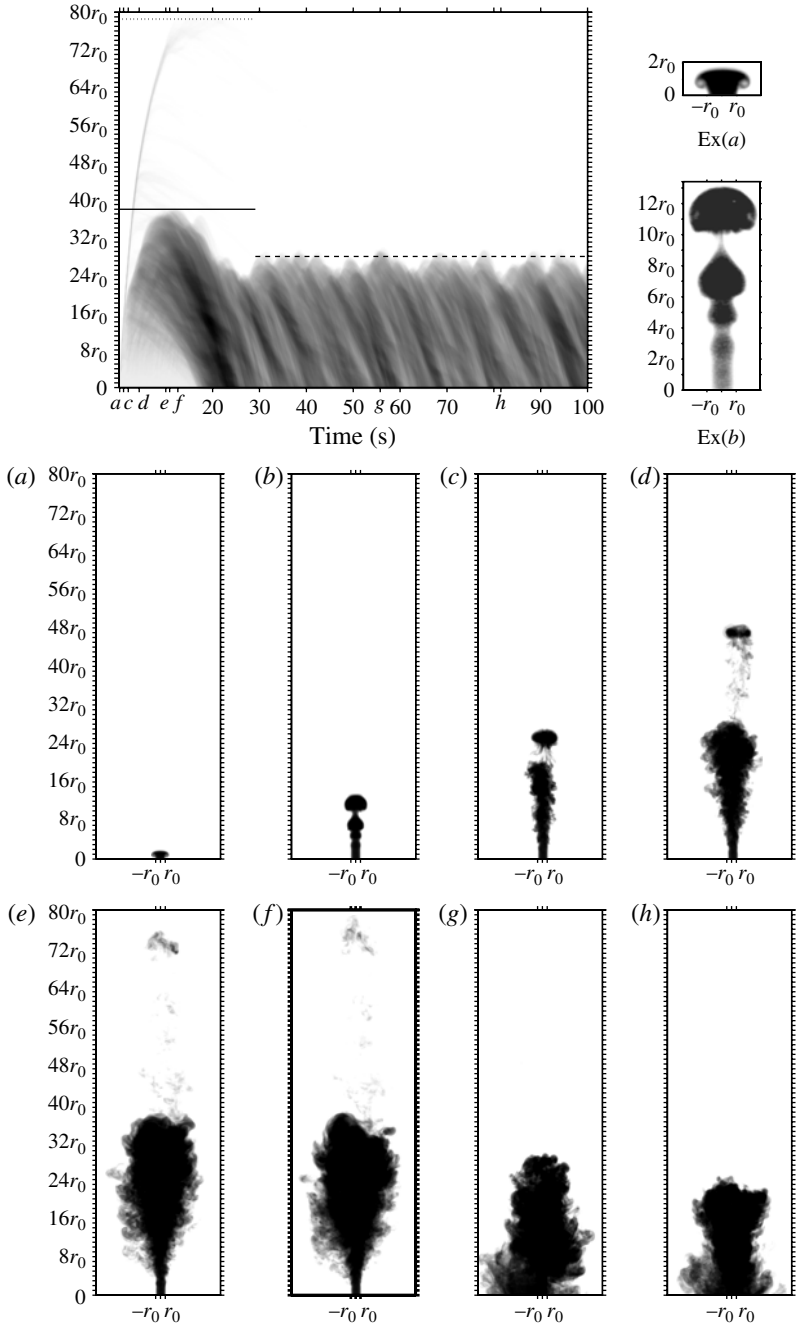

FIGURE 6. Highly forced fountain typical of the class $Fr_0 \gtrsim 5.5$. Time series (top left) and images (*a–h*) for $Fr_0 = 11.9$ and $Re_0 = 2373$. Plotted on the time series are the timing of images (*a*) to (*h*) and the: initial rise height (—), vortex rise height (· · ·) and steady rise height (- - -) for which ($T_1 = 29.2$ s, $T_2 = 343.7$ s). Images Ex(*a*) and Ex(*b*) show exploded sections of images (*a*) and (*b*). Image (*f*) (darker frame) is captured at the initial rise height, $z_f(t) = z_i$.

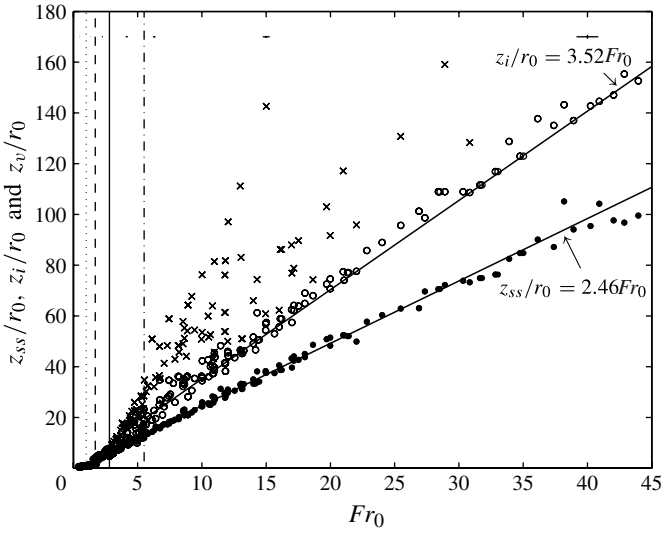

FIGURE 7. Steady z_{ss}/r_0 (•), initial z_i/r_0 (○) and vortex z_v/r_0 (×) rise heights plotted against Fr_0. Seven error bars are plotted at $z/r_0 = 170$.

body subsequently collapsed back and thereafter fluctuated about a reduced (quasi-) steady height, z_{ss}.

The pinched-off vortex continued to rise, reducing in volume on route to attaining a maximum height, z_v. As the vortex decelerated on approach to maximum rise height the decreasing momentum of the vortex by the action of its negative buoyancy became further dampened by viscous effects. The fluid which had formed the vortex evolved into an incoherent negatively buoyant, diffuse cloud-like structure. As this fluid fell back slowly under gravity, weak mixing continued to further dissipate the structure. By the time the cloud fell back to the top of the fountain body it was hardly detectable. On impact the cloud had no discernible effect on the main body of the fountain.

The lower limit of $Fr_0 \approx 5.5$, which we have used to bound the highly forced regime, was the lowest value of Fr_0 for which the lead vortex detached from the body of the fountain. Our results for the steady rise height and the initial rise height (figure 7), and thus the rise height ratio (figure 4 for $Fr_0 \gtrsim 5.5$), fit extremely well with Turner (1966). The solid lines in figures 4 and 7 represent the main findings of Turner (1966), namely that $z_i/r_0 = 3.52Fr_0$, $z_{ss}/r_0 = 2.46Fr_0$ and $\lambda = 1.43$. The best fits to our experimental data are $z_i/r_0 = 3.58Fr_0$, $z_{ss}/r_0 = 2.46Fr_0$ and $\lambda = 1.45$. Whilst these best fits are produced using all our experimental data where $Fr_0 \geqslant 5.5$, the spread in the rise height ratio is considerable for $5.5 \lesssim Fr_0 \lesssim 10$; this results from the difficulty in determining the fountain's initial rise height when the vortex is only just able to separate from the fountain body. The vortex rise heights are discussed in detail in § 3.2.

3.1.2. *Forced fountains,* $2.8 \lesssim Fr_0 \lesssim 5.5$

A rising stem formed with a bulbous cap at its front showing a marked circulation (figure 8*a*). Fluid was periodically ejected downwards from the cap and this fluid descended around the stem as rings centred around the vertical axis of the rising core. The falling rings curled back on themselves (figure 8(*b*) at $z \approx r_0/2$). Smaller

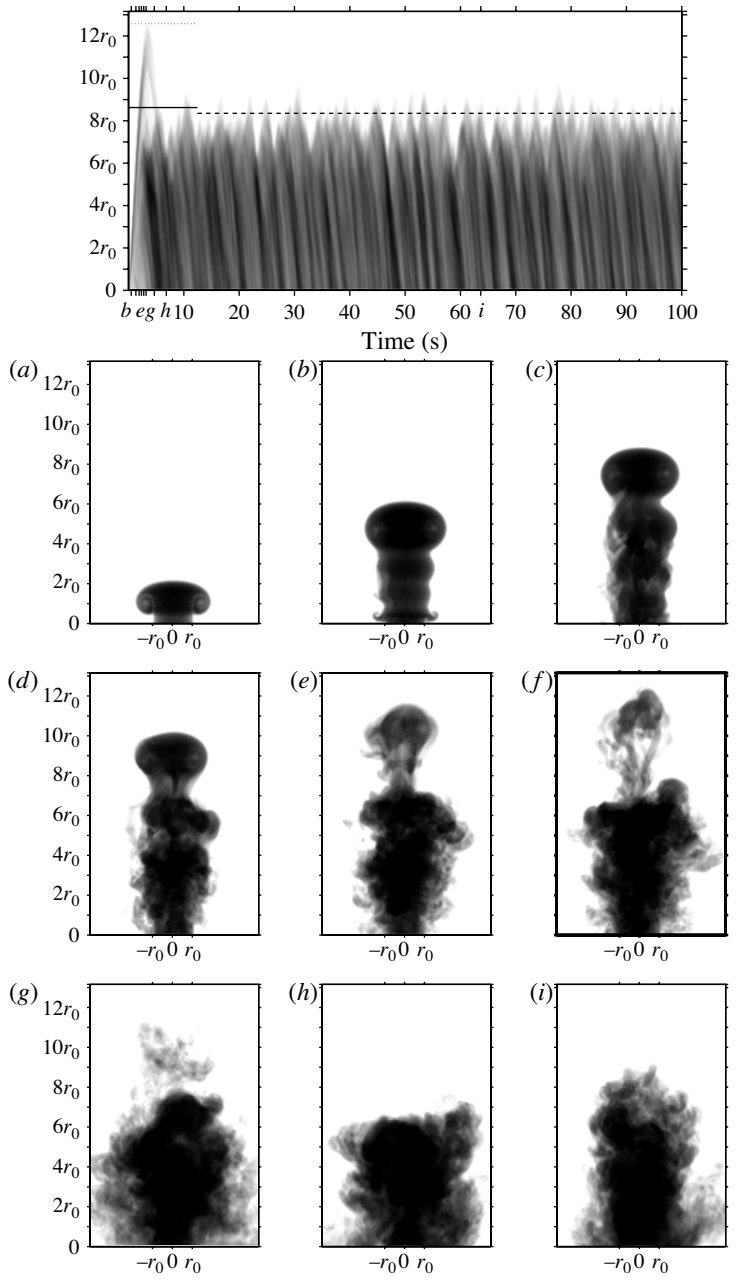

FIGURE 8. Forced fountain typical of the class $2.8 \lesssim Fr_0 \lesssim 5.5$. Time series (top) and images (*a-i*) for $Fr_0 = 3.7$ and $Re_0 = 2166$. Plotted on the time series are the timing of images (*a*) to (*i*) and the: initial rise height (—), vortex rise height (· · ·) and steady rise height (- - -) for which ($T_1 = 12.2$ s, $T_2 = 283.5$ s). Image (*f*) (darker frame) is captured at the initial rise height, $z_f(t) = z_i$.

vortices were advected upwards along the stem, resulting in a ribbed appearance. The falling rings broke up and appeared to introduce instabilities to the fountain's stem (figure 8*c*).

The vortex cap was clearly distinguishable from the main body of the fountain; however unlike releases with $Fr_0 \gtrsim 5.5$ the vortex did not detach (figure 8*e,f*). The volume of the rising vortex was now comparatively larger relative to the fountain body; contrast the scales of the vortex to the fountain in figure 8(*d*) and figure 6(*d*). As the vortex rose fluid fell back from it onto the trailing fountain (figure 8*d–f*) thus suppressing the rise of the fountain body. The body turbulently entrained ambient fluid prior to reaching initial rise height, after which the vortex continued to rise. Fluid falling from the vortex continued to suppress the fountain body as the vortex fell back under gravity and the momentum exchanged between the falling fluid and the fountain body temporarily reduced the fountain's height to a local minimum, which was similar in height to the lowest height subsequently observed once the fountain was in steady state (figure 8*h*). The fountain then rose again to fluctuate around the steady-state rise height.

The rise heights in steady state are well fitted by $z_{ss}/r_0 = 2.46Fr_0$, figure 11. The initial rise height, z_i, of forced fountains is lessened by the presence of fluid falling from the vortex as is evident from the relatively low rise height ratios in figure 14 in § 3.3; this effect is most clearly observed for $Fr_0 \approx 2.8$ (a value marked by the continuous vertical line). For increasing source Froude numbers (within $2.8 \lesssim Fr_0 \lesssim 5.5$) the initial height is less and less affected by the fluid falling from the vortex. As such, for low source Froude number the initial rise height is less than the steady rise height (figure 14). For $Fr_0 \approx 2.8$ we find $\lambda \approx 0.8$, and for increasing Fr_0 the rise height ratio increases towards the constant value $\lambda = 1.45$ as observed for highly forced fountains.

3.1.3. *Intermediate fountains,* $1.7 \lesssim Fr_0 \lesssim 2.8$

The top of the cap rose a number of source radii in height and fluid again wrapped up and circulated within the cap (figure 9*b*). The cap rose atop a stem of fluid which narrowed just beneath the cap to a neck. Towards the lower-Froude-number end of the intermediate fountain range, $Fr_0 \approx 1.7$, the neck occurred immediately above the source whilst towards the upper end, $Fr_0 \approx 2.8$, the cap rose further and additional vortices formed along the stem which developed a ribbed appearance (figure 9*c*). The fountain rose to an initial height, which was the maximum height observed, before slumping back and fluctuating about the lower steady height. Turbulent entrainment was not a feature of intermediate fountains until after the fountain had reached initial rise height (figure 10*d,e*).

The steady rise height is well fitted by the $z_{ss}/r_0 \propto Fr_0^2$ relationship deduced in Kaye & Hunt (2006). For rising Fr_0 in the range $1.7 \leqslant Fr_0 \leqslant 2.8$ the initial rise height increases slightly whilst the rise height ratio, λ, decreases from $\lambda \approx 1.4$ for $Fr_0 \approx 1.7$ to $\lambda \approx 1.0$ for $Fr_0 \approx 2.2$, before increasing to $\lambda \approx 1.3$ for $Fr_0 \approx 2.8$ (figure 14).

3.1.4. *Weak fountains,* $1.0 \lesssim Fr_0 \lesssim 1.7$

The fountain started to rise and then stalled at a height between $r_0 \lesssim z \lesssim 1.5r_0$ either pausing at this height or dipping slightly below it. This stalling forms a local maximum and the initial rise height, z_i, is observed. The fountain then continued to rise to greater heights (figure 5*b*). During the initial rise no circulation was visible within the cap and a neck did not form above the source (contrast images (*b*) of figures 10 and 9).

A symmetrical downflow was observed for a short period after the initial rise height was reached and subsequently the ordered nature of the return flow broke down. Fluid slumped in bulk amounts from the fountain producing an unstable teetering

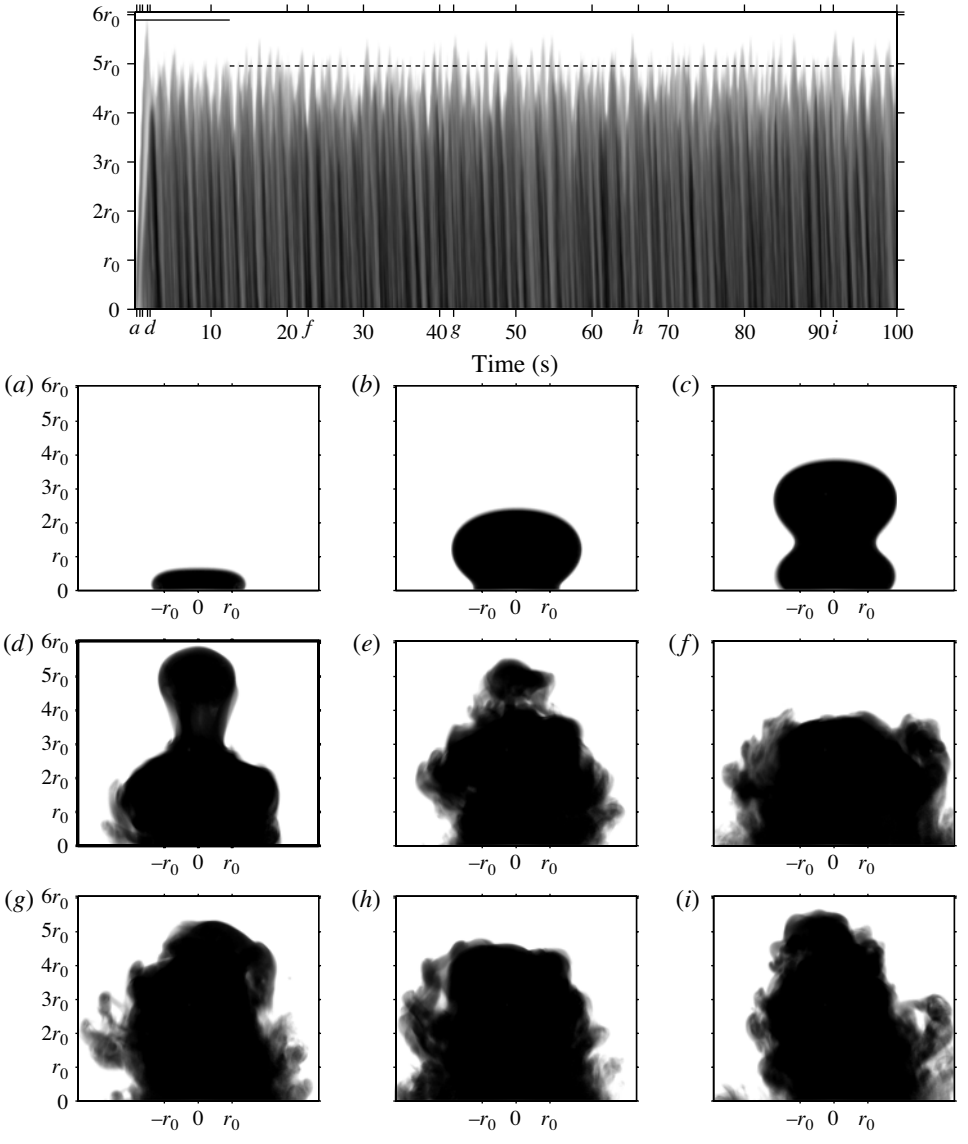

FIGURE 9. Intermediate fountain typical of the class $1.7 \lesssim Fr_0 \lesssim 2.8$. Time series (top) and images (*a–h*) for $Fr_0 = 2.5$ and $Re_0 = 2670$. Plotted on the time series are the timing of images (*a*) to (*h*), the initial rise height (—) and the steady rise height (- - -) for which ($T_1 = 8.2$ s, $T_2 = 233.2$ s). Image (*d*) (darker frame) is captured at the initial rise height, $z_f(t) = z_i$.

appearance. Figure 10(*h* and *i*) and I show a weak fountain in 'steady state', the vast bulk of fluid is above and to the left of the nozzle at the instant the images were captured. Entrainment of ambient fluid into the fountain did occur but to a much lesser extent than for intermediate and forced fountains. Entrainment was only apparent after the fountain had entered (quasi-) steady state. The scaled height fluctuations of weak fountains were approximately double those observed for any other fountain class, with fluctuations in excess of 40 % being observed, figure 15.

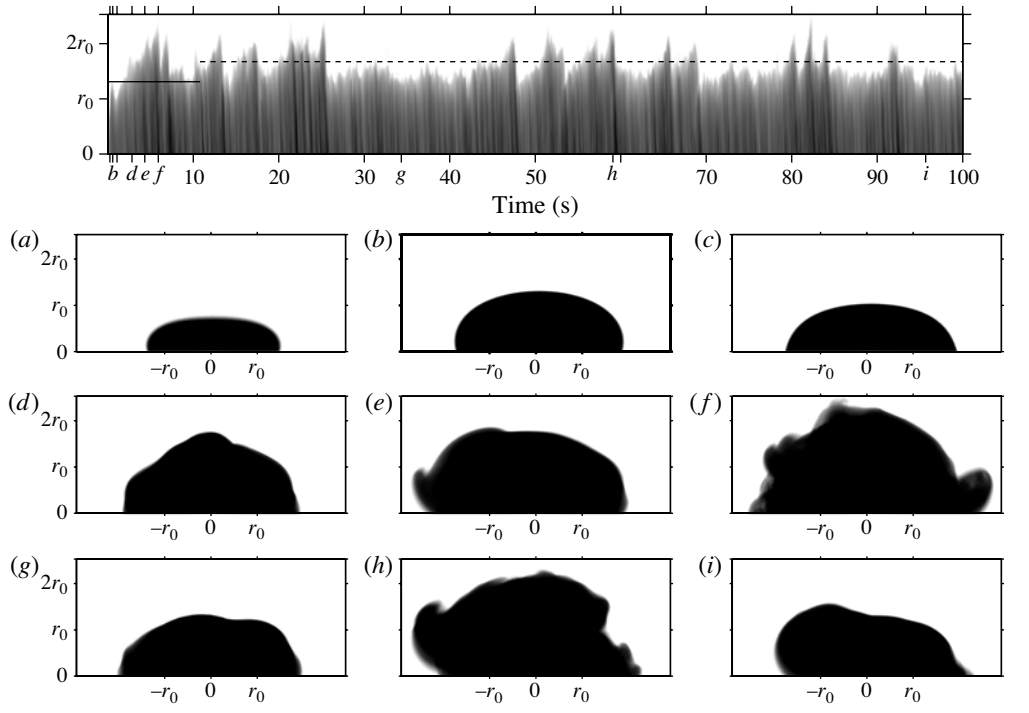

FIGURE 10. Weak fountain typical of the class $1.0 \lesssim Fr_0 \lesssim 1.7$. Time series (top) and images (*a–i*) for $Fr_0 = 1.4$ and $Re_0 = 1891$. Plotted on the time series are the timing of images (*a*) to (*i*), the initial rise height (—) and the steady rise height (- - -) for which ($T_1 = 10.8$ s, $T_2 = 209.7$ s). Image (*b*) (darker frame) is captured at the initial rise height, $z_f(t) = z_i$.

Weak and intermediate fountains exhibit the same dependence of steady rise height on source Froude number, $z_{ss}/r_0 \propto Fr_0^2$, with the best fit to our experimental data being $z_{ss}/r_0 = 0.86Fr_0^2$, (as plotted in figure 11). Increasing Fr_0 across the weak fountain range hardly increases z_i/r_0 whilst λ decreases dramatically (figure 14). The initial rise height is always below the maximum rise height, with initial rise heights as low as half the steady rise height ($\lambda \approx 0.5$ for $Fr_0 \approx 1.7$). This finding was not anticipated, as the steady rise height of a fountain is expected to be less than the initial rise height, given the exchange of momentum between the upflow and the downflow. Based on observation weak fountains do not appear able to form a vortex in the initial rise; however, whilst in steady state these vortices do appear. When formed these vortices significantly increase the fountain height and the failure of the vortex to form in the weak fountain's initial rise leads to the low initial rise heights recorded. Initially the source fluid is ejected into a quiescent ambient whilst subsequently the fluid ejected enters an environment where, due to the prior running of the fountain, there is an induced flow present in the ambient. For weak fountains we argue that the presence or absence of this induced flow is enough to alter whether these vortices are able to form or not – the quiescent ambient appears to dampen the flow so the vortex does not form whilst the presence of the induced flow assists the formation of the vortex. This provides some reasoning for the initial rise height being less than the maximum rise height and explains the scale of height fluctuations observed as the periodic formation

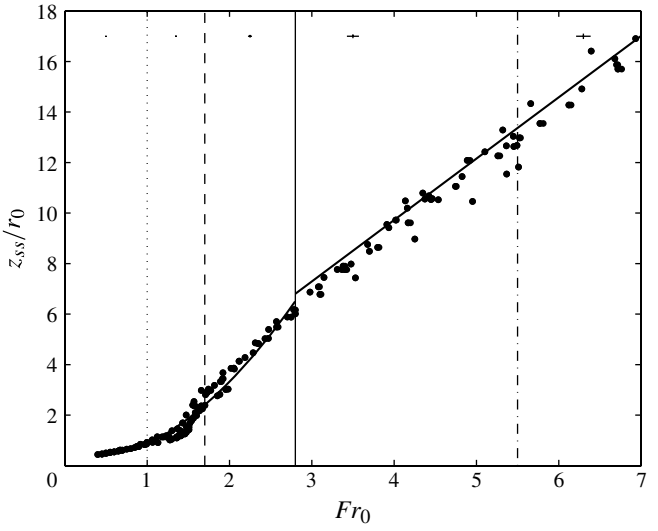

FIGURE 11. Steady rise height z_{ss}/r_0 (•) plotted against Fr_0. The thick solid lines show fits to the Froude number dependences given in Kaye & Hunt (2006), $z_{ss}/r_0 = 0.81Fr_0^{2/3}$ for $0.4 \leqslant Fr_0 \leqslant 1.0$, $z_{ss}/r_0 = 0.86Fr_0^2$ for $1.0 \leqslant Fr_0 \leqslant 2.8$ and $z_{ss}/r_0 = 2.46Fr_0$ for $Fr_0 \geqslant 2.8$. Five error bars are plotted at $z_{ss}/r_0 = 17$.

Class	Fr_0 range	Re_0 range	Steady height dependency
Very weak	0.4–1.0	924–2171	$z_{ss}/r_0 = 0.81Fr_0^{2/3}$
Weak and intermediate	1.0–2.8	1015–2780	$z_{ss}/r_0 = 0.86Fr_0^2$
Forced and highly forced	>2.8	969–4022	$z_{ss}/r_0 = 2.46Fr_0$

TABLE 1. Summary of steady rise height dependence on source Froude number.

of these vortices in steady state would cause the large fountain height fluctuations observed.

3.1.5. *Very weak fountains,* $Fr_0 \lesssim 1.0$

The flow rose to an initial peak height just above the nozzle before collapsing back with an almost symmetrical counterflow. Figure 12(*f*) shows a very weak fountain exhibiting the maximum (albeit small) asymmetry observed for the 32 very weak fountain experiments performed; table 1 in § 4 details the range of Re_0 examined. Whilst the returning flow is not entirely symmetrical, significant downflow is maintained over the entire circumference of the nozzle. There was never any visible entrainment into the fountain. Rise height fluctuations whilst in the steady state are far less than for weak fountains, the scaled height fluctuations being approximately 10 % (figure 15).

The steady rise height agrees well with the $z_{ss}/r_0 \propto Fr_0^{2/3}$ scaling in Kaye & Hunt (2006) and the best fit to our data, $z_{ss}/r_0 = 0.81Fr_0^{2/3}$ is plotted in figure 11. The rise height ratio for very weak fountains is approximately constant at $\lambda \approx 1.2$.

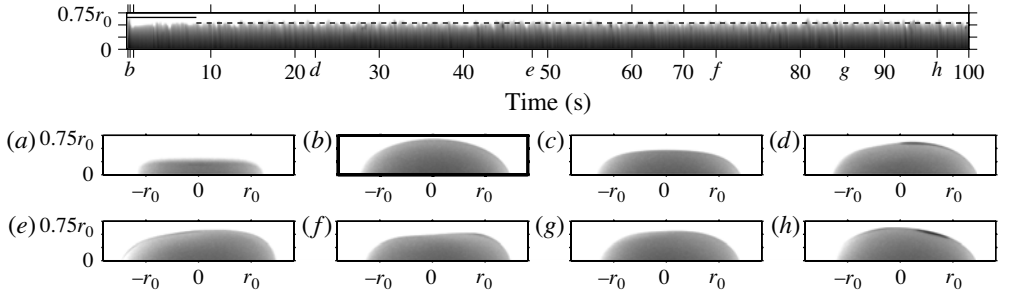

FIGURE 12. Very weak fountain typical of the class $Fr_0 \lesssim 1.0$. Time series (top) and images (*a–h*) for $Fr_0 = 0.7$ and $Re_0 = 1276$. Plotted on the time series are the timing of images (*a*) to (*h*), the initial rise height (—) and the steady rise height (- - -) for which ($T_1 = 4.2$ s, $T_2 = 161.0$ s). Image (*b*) (darker frame) is captured at the initial rise height, $z_f(t) = z_i$.

3.2. *Vortex rise height*

Although not plotted on figure 7, all the maximum vortex rise heights fell below $z_v/r_0 \approx 8Fr_0$ suggesting that the maximum rise height of an 'optimal' vortex, z_{ov}, follows the relationship $z_{ov}/r_0 = 8Fr_0$. Due to the challenges in reproducing z_v consistently, our results demonstrate significant variation beneath this upper bound. This variation was investigated and was found not to result from changes in the source conditions over the ranges (table 1) of Fr_0 and Re_0 investigated.

Successful formation of a vortex required a rapid initial acceleration of the source fluid and a sharp density interface at the nozzle exit. Considerable efforts were made to maximise the occurrence of an 'optimal' vortex by monitoring the ramp-up time, t_r/t_i, along with the diffusive and settling time scales; procedural details are provided in § 2.3 and these ensured our experiments provided repeatable fountain dynamics and repeatable vortex formation. This was confirmed by a repeatability study on six fountains all of $Fr_0 = 10.0$. This included three fountains of nominally identical source conditions and three fountains of varied r_0, w_0 and g_0' so that the source Reynolds number was altered between the three experiments, $1343 \leqslant Re_0 \leqslant 3212$. Taking the coefficient of variation as a measure of spread between the six experiments, z_{ss} varied by less than 3 %, z_i by less than 4 %, yet z_v was found to vary by more than 20 %. Moreover, the heights z_{ss}, z_i and z_v all showed no sensitivity to Re_0. As a further indicator of the repeatability of the initial formation and rise of the vortex we examined the height at which the vortex pinched off from the fountain body; this height varied by less than 5 %.

Thus the majority of the spread in the results of z_v (figure 7) cannot be attributed to the source conditions directly but to disturbances influencing the vortex after pinch-off. These disturbances are likely to grow from those initiated during pinch-off or from weak disturbances in the ambient. The vortex would often ride atop the fountain to heights of around $30r_0$ before separating from the main body (figure 6*c*) and post separation the vortex travelled to heights of up to $140r_0$ (figure 7). The large distances travelled, combined with the diffuse nature of the fluid when high above the fountain body (figure 6*f*) allowed any fractional disturbance to influence the vortex. Any disturbance in the pinched-off vortex caused it to depart from a vertical trajectory or to break up prior to attaining the rise height of an optimally formed vortex, z_{ov}.

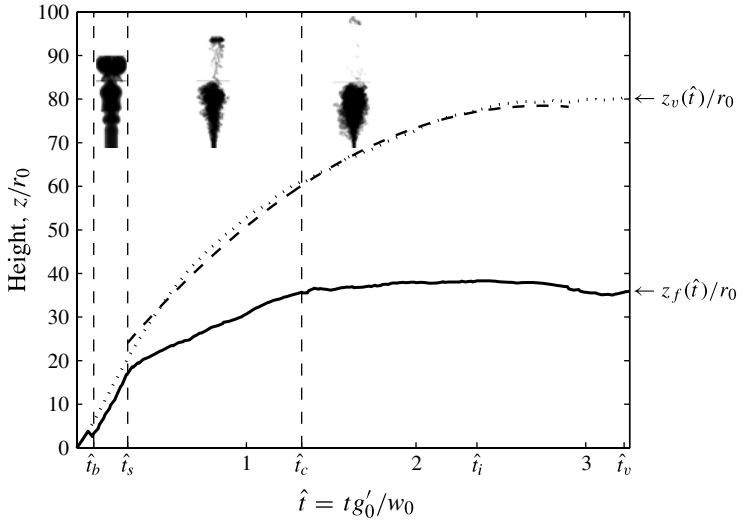

FIGURE 13. Fountain body front $z_f(\hat{t})/r_0$ (—) and vortex $z_v(\hat{t})/r_0$ ($\cdots$) rise heights plotted against time for a typical highly forced fountain. Times indicated are of: the appearance of a distinct fountain body and vortex, $\hat{t}_b$; the vortex separation, $\hat{t}_s$; the commencement of the downflow, $\hat{t}_c$; the maximum initial rise height, $\hat{t}_i$, and of the maximum vortex rise height, $\hat{t}_v$. The three superimposed images of the fountain are located at their times of capture. The source conditions of the fountain pictured were: $Fr_0 = 11.8$, $w_0 = 21.1$ cm s^{-1}, $g_0' = 4.2$ cm s^{-2} and $r_0 = 0.8$ cm. The path of a projectile of parabolic form $z = c_1 w_0 t - c_2 g_0' t^2$, where the coefficients were determined by a least-squares fit to the actual path of the separated vortex, is illustrated (- - -).

Figure 13 plots the vertical position of the vortex top and fountain body top against scaled time ($\hat{t} = tg_0'/w_0$) for a single fountain. The behaviour shown is typical of highly forced fountains. The rise of the separated vortex is well predicted by modelling it as a projectile. We denote the time at which the height of the fountain body becomes distinguishable from the vortex height as $\hat{t} = \hat{t}_b$ ($\approx$0.1 in figure 13) and the time the vortex separates from the fountain body as $\hat{t}_s$. Figure 13 shows the potential to divide the evolution of $z_f(\hat{t})$ into three distinct regions. For $\hat{t}_b \leqslant \hat{t} \leqslant \hat{t}_s$ the vortex and the body rise at the same near-constant velocity. During this initial development the vortex dominates the rise of the fountain; note that at $\hat{t} = \hat{t}_b$ the vortex velocity is unchanged and the fountain-top velocity is that of the vortex. The beginning of the second region, $\hat{t}_s \leqslant \hat{t} \leqslant \hat{t}_c$, is marked by a clear decrease in the gradient of $z_f(\hat{t})$, which corresponds to an increased vertical separation between the fountain-top, $z_f(\hat{t})$, and the vortex, $z_v(\hat{t})$. The end of the second region, at $\hat{t} = \hat{t}_c$, corresponds to the time at which the development of the counterflow commences. Within the third region, $\hat{t}_c \leqslant \hat{t} \leqslant \hat{t}_i$, the fountain-top continues to decelerate as it rises towards the initial maximum height, z_i.

3.3. *Weak to intermediate fountains, $Fr_0 \approx 1.7$, and the λ jump*

The transition from weak to intermediate fountains on increasing Fr_0 is marked by a sudden jump in the initial rise height at $Fr_0 \approx 1.7$, a jump which causes the rise height ratio to increase suddenly from $\lambda \approx 0.5$ to $\lambda \approx 1.5$ (figure 14). This step change in λ is the result of the physics of the fountain's initial rise. This is in contrast to the

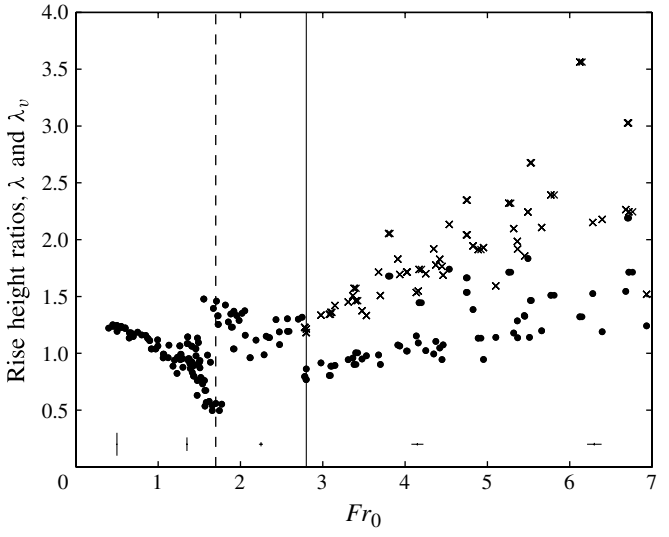

FIGURE 14. Rise height ratios λ (•) and λ_v (×) plotted against Fr_0. Five error bars are plotted at λ=0.2.

other apparent step change in rise height ratio at $Fr_0 \approx 2.8$, which results only from the onset of recording the vortex height and fountain height separately.

The jump in λ, at $Fr_0 \approx 1.7$, is driven by a sudden change in the initial rise height, z_i (note that figure 11 shows the steady-state height continuously increasing over the range of $1.5 \leqslant Fr_0 \leqslant 2.0$). We hypothesise that this step change in the initial rise height results from the source forcing being just sufficient to form a vortex. As a consequence the fluid released wraps up above the nozzle, increasing the rise height, rather than spilling over the nozzle perimeter. Gharib, Rambod & Shariff (1998) report the formation number of neutrally buoyant vortices as $L/D \approx 4$, L denoting the length and D the diameter of a column of fluid which comprises the volume of the starting vortex. The volume of this column is then $8\pi r_0^3$. Given that both weak and intermediate fountains show no signs of entrainment during their initial rise we might expect this volume of fluid to be the volume of the initial vortex. A torus of minor radius r_t and major radius r_t is the likely shape of the initial vortex and this would contain a volume of fluid $2\pi^2 r_t^3$. Setting the two volumes to be equal gives $r_t/r_0 = (4/\pi)^{1/3} \approx 1.08$. Given this, the height of the torus would be $2r_t = 2.16r_0$. Should the initial rise of the fountain exceed $2.16r_0$ the vortex can form above the height of the nozzle whilst if the initial rise of the fountains is below $2.16r_0$ the circulation of the vortex would be interrupted by the external wall of the nozzle. The λ jump at $Fr_0 \approx 1.7$ corresponds to a change in the initial rise height from $z_i \approx 1.8r_0$ to $z_i \approx 3.5r_0$ spanning the height $2.16r_0$. This indicates that once the fountain reaches a height close to $2.16r_0$ the formation of the vortex allows the fountain to attain much greater initial rise heights and thus supports the claim that the λ jump is caused by the successful formation of an initial vortex.

3.4. *Fountain height fluctuations*

The fluctuation of fountain height in steady state (scaled on the mean steady height) was found to be a maximum for weak fountains, $1.0 \lesssim Fr_0 \lesssim 1.7$, which agrees well with the results of Friedman (2006). Figure 15 plots the scaled height fluctuation

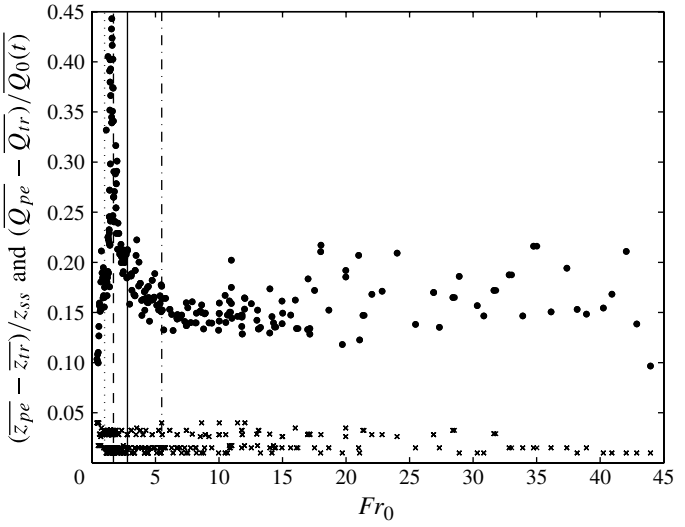

FIGURE 15. Rise height fluctuations $(\overline{z_{pe}} - \overline{z_{tr}})/z_{ss}$ (•) and source volume flux fluctuations $(\overline{Q_{pe}} - \overline{Q_{tr}})/\overline{Q(t)}$ (×) plotted against Fr_0.

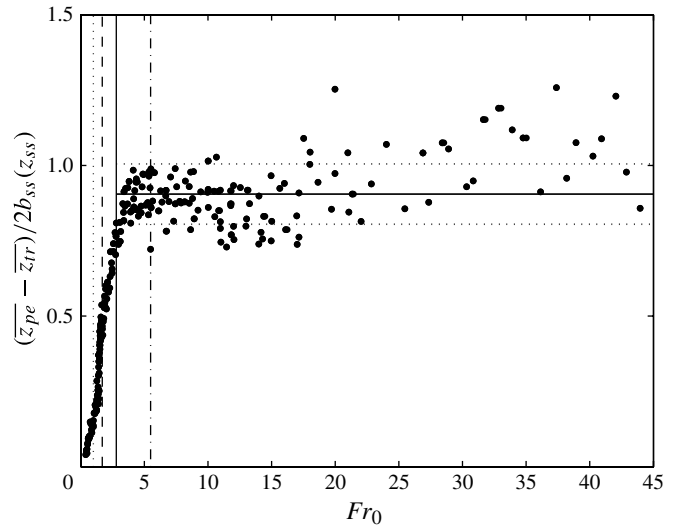

FIGURE 16. Mean rise height fluctuations scaled on steady fountain width plotted against Fr_0. The horizontal solid line $\overline{(\overline{z_{pe}} - \overline{z_{tr}})/2b_{ss}(z_{ss})} = 0.92$ is the mean value for $Fr_0 \geqslant 2.8$ (i.e. for forced fountains). The dotted horizontal lines represent 10 % above and below the mean.

against Fr_0 and shows that for $Fr_0 \gtrsim 5.5$ fluctuations are independent of Fr_0, i.e. as these are relatively highly forced fountains (for which $z_{ss}/r_0 \propto Fr_0$) the absolute height fluctuations scale linearly with Fr_0. Also plotted in figure 15 are the variations in source volume flow rate, Q_0, associated with each experiment. The variation in Q_0 shows no correlation with the height fluctuations and we can conclude that the fluctuations were not caused by variations in the volume flow rate.

The cause of the dominant height fluctuations is expected to be large-scale eddies periodically forming at the top of the fountain. We expect the scale of these fluctuations, $\overline{z_{pe}} - \overline{z_{tr}}$, to be comparable with the scale of the largest eddy able to form at the top of the fountain, the length scale of this eddy being the width of the fountain-top.

Figure 16 plots the height fluctuations, $\overline{z_{pe}} - \overline{z_{tr}}$, scaled on fountain-top width, $2b_{ss}(z_{ss})$. For $Fr_0 \geqslant 2.8$ the plot illustrates that $(\overline{z_{pe}} - \overline{z_{tr}})/2b_{ss}(z_{ss})$ shows no clear dependence on Fr_0 with the mean value being $(\overline{z_{pe}} - \overline{z_{tr}})/2b_{ss}(z_{ss}) = 0.92$ and over 70 % of all experiments falling within 10 % of this mean value. This demonstrates that for fountains of $Fr_0 \geqslant 2.8$ the scale of fountain height fluctuations is approximately the fountain-top width, thus supporting the proposal that large-scale eddies at the fountain-top are the dominant cause of fountain height fluctuations.

4. Discussion

Our measurement of saline fountains support the experimental and theoretical work of previous studies (for example Turner 1966; Baines *et al.* 1990; Kaye & Hunt 2006). Our study, in addition to providing a substantial dataset which clarifies previous results, also highlights new rise height behaviours. The steady-state rise height dependence across the range of source Froude numbers investigated ($0.4 \leqslant Fr_0 \leqslant 45$) are summarized in table 1. The new rise height behaviours have identified the need to classify axisymmetric turbulent fountains into five regimes based on the dynamics of the initial transients and those of the (quasi-) steady state. The rise height ratio was found to vary by a factor of four (figure 14) with the trends for each of the five fountain classes detailed in table 2.

An exhaustive study of the effects of Re_0 on λ was not carried out as the intention of this study was to examine fountains of sufficiently high Re_0 that both z_i and z_{ss} were insensitive to Re_0. However, the fountains studied did vary in source Reynolds number over a relatively wide range, detailed in table 1. For the entire range of Fr_0 and Re_0 examined the steady rise height was found to be insensitive to Re_0 (§ 2.3). Furthermore, this was also the case for the initial rise heights of the very weak, forced and highly forced fountains studied (§ 3.2). For weak and intermediate fountains close to the transitional value of $Fr_0 \approx 1.7$ the formation, or otherwise, of the initial vortex was found to be affected by Re_0. This in turn affected the initial rise height attained and thus λ. The formation of the initial vortex and its dependence on Re_0 is apparent within figure 14 through the overlapping trends in λ at $Fr_0 \approx 1.7$. This transitional value of λ may itself be sensitive to Re_0. These transitional fountains form the basis of an ongoing study.

Weak fountains stall on their initial rise yielding an initial maximum height lower than the maximum rise heights observed once in steady state. We argue this is due to the failure of a vortex to form during the initial rise thus reducing the initial rise height, whilst the successful formation of the vortex in steady state occurs periodically thus producing the elevated heights observed in steady state. In the steady state, these weak fountains experience height fluctuations of approximately $0.4z_{ss}$, this being around twice the magnitude of fluctuations observed for any other fountain class.

The fact that for highly forced fountains, a vortex forms at the fountain's front which pinches off, separates from and then rises high above the fountain body, changes the dynamics of the initial transients compared with fountains of lower Fr_0 and adds an additional rise height (the vortex rise height) to consider. The sensitivity of this vortex to the initial conditions in the nozzle, the acceleration profile of the

Class	Fr_0 range	λ (low and high Fr_0)	Trend for increasing Fr_0	Relative rise heights
Very weak	0.4–1.0	1.1 and 1.0	Approximately constant	$z_i \geqslant z_{ss}$
Weak	1.0–1.7	1.0 and 0.5	Strongly decreasing	$z_i \leqslant z_{ss}$
Intermediate	1.7–2.8	1.4 and 1.3	Decreasing (to $\lambda \approx 1.0$) then increasing	$z_i > z_{ss}$
Forced	2.8–5.5	1.0 and 1.45	Weakly increasing	$z_i \geqslant z_{ss}$, $z_v > z_i$
Highly forced	5.5–45	1.45 and 1.45	Constant	$z_i > z_{ss}$, $z_v > z_i$

TABLE 2. Summary of rise height ratio, λ, trends for the five fountain classes.

pump and any residual motion in the ambient conditions make detailed analysis challenging. Our results for the vortex height are well bounded by an upper limit of $z_v/r_0 \leqslant 8Fr_0$ but demonstrate significant variation below this limit. The initial vortex is also visible in both intermediate and forced fountains. Whilst for these fountains the vortex fails to separate, its presence plays a central role in the transients. Given the number of previous studies of turbulent fountains it is perhaps surprising to find so few references to vortices separating from the fountain's front. Moreover, few previous studies of fountains provide details of the initial acceleration of the source fluid. Notably, Marugán-Cruz *et al.* (2009) in their study of laminar starting fountains analysed the initial accelerations achieved and observed the initial vortex separating.

5. Conclusions

For fountains of $Fr_0 \gtrsim 2.8$ (i.e. forced and highly forced) our results show the dominant scale of the height fluctuations to be approximately the width $2b_{ss}(z_{ss})$ of the fountain near its top. The width $2b_{ss}(z_{ss})$ is also the characteristic length scale of the largest eddying motion able to form in this region. Thus we conclude that large-scale eddies periodically forming at the fountain-top are the dominant cause of fountain height fluctuations in the (quasi-) steady state.

We conclude it is inappropriate to consider the rise height ratio constant at $\lambda = 1.43$ except for highly forced fountains. In order to clarify the rise height behaviours of axisymmetric turbulent Boussinesq fountains we have classified them into five fountain classes, see table 2.

This work was motivated, in part, by Carazzo *et al.* (2010) highlighting the lack of data on the variation, or otherwise, of the rise height ratio with Fr_0 and so we finish by considering the implications of our measurements for the results of their model, specifically that $\lambda = z_i/z_{ss} \propto \sqrt{\alpha_{ss}/\alpha_i}$. Our results show that $\lambda = \mathrm{f}(Fr_0)$, see figure 4, which in turn requires that $\alpha_{ss}/\alpha_i = \mathrm{f}(Fr_0)$. Whether the variation in the ratio of entrainment coefficients with Fr_0 is sufficient to alone account for the wide variation observed in λ, a variation by a factor of four, remains an open question as the ratio of entrainment coefficients would be required to vary by a factor of sixteen.

Considering highly forced fountains, $\alpha_i \approx \alpha_{jet}$ as fluid projected is jet-like over the majority of the initial rise height (see the Appendix). Furthermore, the projected fluid reaches relatively large rise heights before falling as a plume with zero source momentum flux so that entrainment by the falling fluid can be assumed similar to that of a pure plume, i.e. $\alpha_{ss} \approx \alpha_p$. Finally, as we determined that, for these fountains, $\lambda = 1.45$ we can write $1.45 \propto \sqrt{\alpha_{ss}/\alpha_i}$. Taking $\alpha_i \approx \alpha_{jet} = 0.0535$ (Fischer *et al.* 1979) and $\alpha_{ss} \approx \alpha_p = 0.0833$ (Fischer *et al.* 1979) we have $\lambda = z_i/z_{ss} \approx 1.16\sqrt{\alpha_{ss}/\alpha_i}$.

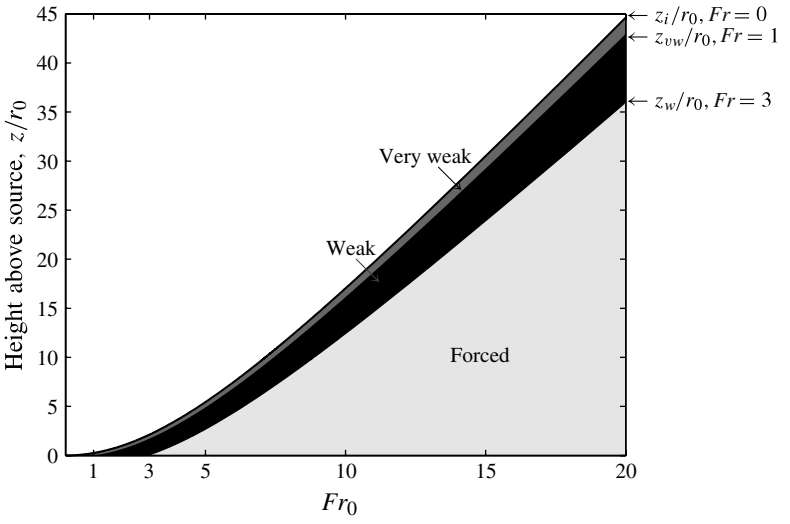

FIGURE 17. Contours of constant Froude number showing the vertical height at which: (i) $Fr = 0$, i.e. the initial rise height, z_i; (ii) $Fr = 1$, marking the transition from weak to very weak, z_{vw}; and (iii) $Fr = 3$, marking the transition from forced to weak, z_w. The relative vertical extents of the three shaded regions for a given Fr_0 indicate the fraction of the initial rise height from (A 1) over which the Froude number is locally forced, weak and very weak.

Acknowledgement

H.C.B and G.R.H gratefully acknowledge the technical support of W. Bobinski and D. De Ruyter and the funding provided by the EPSRC.

Appendix. Relative fountain height at transitional local Froude numbers

The relative contribution of the three length scales to the overall initial fountain rise height (Kaye & Hunt 2006, their equation (2.8)) may be expressed as

$$\frac{z_i}{r_0} = A\int_{Fr_0}^{0} B(F)\,\mathrm{d}F = \underbrace{A\int_{Fr_0}^{Fr_w} B(F)\,\mathrm{d}F}_{z_w/r_0} + \underbrace{A\int_{Fr_w}^{Fr_{vw}} B(F)\,\mathrm{d}F}_{(z_{vw}-z_w)/r_0} + \underbrace{A\int_{Fr_{vw}}^{0} B(F)\,\mathrm{d}F}_{(z_i-z_{vw})/r_0} \quad \text{(A 1)}$$

where $A = (2a/5)Fr_0\,(\phi + aFr_0^{-2})^{3/10}$, $B(F) = F^{-2}\,(\phi + aF^{-2})^{-13/10}$ and $a = 5\pi^{1/2}/4\alpha$.

To obtain estimates of the relative heights to which a forced fountain rises before the local Froude number decreases to values associated with a weak fountain, z_w, and a very weak fountain, z_{vw} (the remaining rise height, $z_i - z_{vw}$, being the height gained whilst the local Froude number is equivalent to those very weak fountains), we take the transitional Froude numbers of $Fr_w = 3$ and $Fr_{vw} = 1$, respectively, with $\phi = \alpha/\alpha_{jet} = 1$ (Kaye & Hunt 2006). The heights z_w, z_{vw} and z_i scaled on the source radius are illustrated in figure 17 for source Froude numbers spanning the three fountain regimes. The plot highlights that for sufficiently highly forced fountains it is the contribution of the momentum-jet length that dominates the initial rise height.

REFERENCES

ANSONG, J. K., KYBA, P. J. & SUTHERLAND, B. R. 2008 Fountains impinging on a density interface. *J. Fluid Mech.* **595**, 115–139.

BAINES, W. D., TURNER, J. S. & CAMPBELL, I. H. 1990 Turbulent fountains in an open chamber. *J. Fluid Mech.* **212**, 557–592.

BLOOMFIELD, L. J. & KERR, R. C. 1998 Turbulent fountains in a stratified fluid. *J. Fluid Mech.* **358**, 335–356.

BLOOMFIELD, L. J. & KERR, R. C. 2000 A theoretical model of a turbulent fountain. *J. Fluid Mech.* **424**, 197–216.

CAMPBELL, I. H. & TURNER, J. S. 1989 Fountains in magma chambers. *J. Petrol.* **30**, 885–923.

CARAZZO, G., KAMINSKI, E. & TAIT, S. 2010 The rise and fall of turbulent fountains: a new model for improved quantitative predictions. *J. Fluid Mech.* **657**, 265–284.

DEVENISH, B. J., ROONEY, G. G. & THOMPSON, D. J. 2010 Large-eddy simulation of a buoyant plume in uniform and stably stratified environments. *J. Fluid Mech.* **652**, 75–103.

FISCHER, H. B., LIST, E. J., KOH, R. C. Y., IMBERGER, J. & BROOKS, N. H. 1979 *Mixing in Inland and Coastal Waters*. Academic.

FRIEDMAN, P. D. 2006 Oscillation in height of a negatively buoyant jet. *Trans. ASME: J. Fluids Engng* **128**, 880–882.

FRIEDMAN, P. D. & KATZ, J. 1999 The flow and mixing mechanisms caused by the impingement of an immiscible interface with a vertical jet. *Phys. Fluids* **11**, 2598.

GHARIB, M., RAMBOD, E. & SHARIFF, K. 1998 A universal time scale for vortex ring formation. *J. Fluid Mech.* **360**, 121–140.

KAYE, N. B. & HUNT, G. R. 2006 Weak fountains. *J. Fluid Mech.* **558**, 319–328.

LIN, W. & ARMFIELD, S. W. 2000*a* Direct simulation of weak axisymmetric fountains in a homogeneous fluid. *J. Fluid Mech.* **403**, 67–88.

LIN, W. & ARMFIELD, S. W. 2000*b* Very weak fountains in a homogeneous fluid. *Numer. Heat Transfer* A **38**, 377–396.

LIU, Q. A. & LINDEN, P. F. 2006 The fluid dynamics of an underfloor air distribution system. *J. Fluid Mech.* **554**, 323–341.

MARUGÁN-CRUZ, C., RODRÍGUEZ-RODRÍGUEZ, J. & MARTÍNEZ-BAZÁN, C. 2009 Negatively buoyant starting jets. *Phys. Fluids* **21**, 1–14.

MCDOUGALL, T. J. 1981 Negatively buoyant vertical jets. *Tellus* **33**, 313–320.

MORTON, B. R., TAYLOR, G. I. & TURNER, J. S. 1956 Turbulent gravitational convection from maintained and instantaneous sources. *Proc. R. Soc. Lond.* A **234**, 1–23.

TENNEKES, H. & LUMLEY, J. L. 1972 *A First Course in Turbulence*. MIT.

TURNER, J. S. 1966 Jets and plumes with negative or reversing buoyancy. *J. Fluid Mech.* **26**, 779–792.

WANG, R.-Q. W., LAW, A. W.-K. & ADAMS, E. E. 2011 Pinch-off and formation number of negatively buoyant jets. *Phys. Fluids* **23**, 52101.

WASHBURN, E. W. (Ed.) 2003 *International Critical Tables of Numerical Data, Physics, Chemistry and Technology*. Knovel.

WHITE, F. J. 2003 *Fluid Mechanics*. McGraw-Hill.

WILLIAMSON, N., ARMFIELD, S. W. & LIN, W. 2010 Transition behaviour of weak turbulent fountains. *J. Fluid Mech.* **655**, 306–326.

WILLIAMSON, N., ARMFIELD, S. W. & LIN, W. 2011 Forced turbulent fountain flow behaviour. *J. Fluid Mech.* **671**, 535–558.

WILLIAMSON, N., SRINARAYANA, N., ARMFIELD, S. W., MCBAIN, G. D. & LIN, W. 2008 Low-Reynolds-number fountain behaviour. *J. Fluid Mech.* **608**, 297–317.

ZHANG, H. & BADDOUR, R. E. 1998 Maximum penetration of vertical round dense jets at small and large Froude numbers. *J. Hydraul. Engng* **124**, 550–553.